Supplementary Information

An active $Ni(OH)_2/MnCO_3$ catalyst with efficient synergism for alkaline methanol oxidation

Chunru Liu[a], Fulin Yang[a], Yun Yang[b]*, Shuli Wang[a], Ligang Feng*[a]

[a] School of Chemistry and Chemical Engineering, Yangzhou University, Yangzhou 225002, P.R China.

E-mail: ligang.feng@yzu.edu.cn, fenglg11@gmail.com

b.Nanomaterials and Chemistry Key Laboratory, Wenzhou University, Wenzhou, P. R. China. E-mail: bachier@163.com

Experimental sections

Chemicals and materials

Chemicals

All the reagents in the experiment were analytical grade and used as received. Nickel nitrate hexahydrate ($Ni(NO_3)_2 \cdot 6H_2O$), Manganese nitrate tetrahydrate ($Mn(NO_3)_2 \cdot 4H_2O$), Sodium carbonate (Na_2CO_3), and Potassium hydroxide (KOH) were purchased from Shanghai Aladdin Bio-Chem Technology Co., Ltd. Nafion (5 wt%) was purchased from Sigma-Aldrich. All solutions were prepared with ultrapure water with a resistance of 18.2 MΩ (Thermo Fisher Scientific (USA) Co., Ltd).

Preparation of the catalysts

The typical procedure was as follows: Solution (A) contained the precalculated volume (15 mL) of metal nitrates of 1 mol L^{-1} $Ni(NO_3)_2 \cdot 6H_2O$ and (0.5, 0.33, 0.25) mol/L $Mn(NO_3)_2 \cdot 4H_2O$. The solution (B), containing the precipitating agent (1 mol L^{-1} NaOH + 0.5 mol L^{-1} Na_2CO_3 with a volume ratio of 1), was added simultaneously into a 250 mL three-necked round flask, where the pH value was kept around 10 under the vigorous stirring at room temperature. The obtained slurry was further aged for 6 h. Subsequently, the aged slurry was further transferred into a Teflon-lined autoclave and hydrothermally treated at 120 ℃ for 6 h. The finally obtained hybrid oxide catalysts were denoted as $Ni(OH)_2/MnCO_3$(2:1), $Ni(OH)_2/MnCO_3$(3:1) and $Ni(OH)_2/MnCO_3$(4:1), respectively. The same preparation method was used to prepare $Ni(OH)_2$ and $MnCO_3$, the only difference was that solution (A) only contained 1 mol L^{-1} of Ni^{2+} or Mn^{2+}.

Physical characterization

Powder X-ray diffraction (XRD) patterns were tested on a Bruker D8 Advance powder X-ray diffractometer using a Cu K_α (λ=1.5405 Å) radiation source operating at 40 kV and 40 mA and at a scanning rate of 5° min^{-1}. The morphology and microstructure were analyzed by Field Emission Scanning Electron Microscope (FESEM, Hitachi, S-4800 II, Japan). All transmission electron microscopy (TEM) and high-resolution TEM (HRTEM) measurements were conducted on a TECNAI G2 operating at 300 kV. The energy-dispersive X-ray detector spectrum (EDS) was

obtained on a TECNAI G2 transmission electron microscope equipped with an EDXA detector. All X-ray photoelectron spectroscopy (XPS) measurements were carried out on Kratos XSAM-800 spectrometers with an Al K_α radiation source.

Electrochemical Pre-treatment

All the electrochemical measurements are carried out with a Bio-Logic VSP electrochemical workstation (Bio-Logic Co., France) and a conventional three-electrode system. The working electrode is a glassy carbon electrode (3 mm diameter, 0.07 cm^2). The graphite rod and the saturated calomel electrode (SCE, Hg/Hg_2Cl_2) serve as a counter and a reference electrode through a double salt bridge and lugging capillary tip, the potential was carefully checked before and after the relevant measurements. The potentials reported in the work were converted to the reversible hydrogen electrode (RHE), E(RHE) = E(SCE) + 0.0591*pH + 0.242 V. The catalyst ink was prepared by ultrasonically dispersing a mixture containing 4.5 mg of catalyst and 0.5 mg of carbon black, 950 μL of ethanol, and 50 μL of a 5 wt% Nafion solution. Next, pipette 10 μL of the catalyst ink onto a pre-cleaned working electrode, and then clamp the electrode with the electrode clip to start the test.

Electrochemical measurements

The cyclic voltammetry (CV) curves of all catalysts were recorded in 1 M KOH solution or 1 M KOH + 1 M CH_3OH solution with the potential range from 0 to 0.8 V *vs.* SCE (1.06 to 1.86 V *vs.* RHE). The current density was obtained by normalizing the current to the geometric surface. No iR-compensation was applied to the methanol oxidation measurement.

Tafel slope analysis

The overpotential values are defined by the Tafel equation: $\eta = a + b\log|j|$, where η (V) is the overpotential, j (mA cm^{-2}) is the current density; b (mV dec^{-1}) represents the Tafel slope.

Electrochemical Impedance Spectroscopy (EIS) analysis

The ohmic resistance used for iR-compensation was obtained from electrochemical impedance spectroscopy measurements with frequencies ranging from 1000 kHz to 10 mHz with an amplitude of 5 mV.

ECSA measurements and calculation

The electrochemical surface area (ECSA) was evaluated in terms of double-layer capacitance (C_{dl}). The ECSA was estimated by CV without Faradaic processes occurred region from -0.02 to

0.1 V *vs*. SCE (1.04 to 1.16 V *vs.* RHE) in 1 M KOH at scan rates of 20, 40, 60, 80, and 100 mV s^{-1}. The C_{dl} was estimated by plotting the △J = (Ja - Jc)/2 at 0.04 V *vs*. SCE (1.1 V *vs.* RHE) against the scan rate. The linear slope is the double-layer capacitance C_{dl}. The specific capacitance is evaluated for a flat surface by assuming 40 μF cm^{-2} according to previous literature. The electrochemically active surface area was achieved by normalizing the double-layer capacitance to the standard specific capacitance. The roughness factor (R_f) can be calculated by (ECSA) based on the geometric surface area of the electrode (0.07 cm^2).

Specific activity and Turnover frequency (TOF)

The specific activity was obtained by normalizing the apparent current to ECSA. The TOF (s^{-1}) for MOR analysis can be calculated with the following equation TOF = I/(6*F*n). Where I is the current (A) during linear sweep measurement, F is the Faraday's constant (96500 C/mol), and n is the number of active sites (mol). The factor 1/6 is based on the consideration that six electrons are required to consume one molecule of methanol. Herein, all the Ni metal atoms on the electrode are assumed to be the active sites. And the amount of the Ni in the electrode is known and the molar amount of the Ni can be calculated according to the formula: n (mol) = catalyst loading on the glassy carbon electrode*metal content/molar mass of metal.

Stability test and Chronoamperometry (CA) measurements

To estimate the stability of all samples except Pt/C (20 wt%), the chronoamperometry (CA) was performed at a potential of 0.5 V *vs*. SCE (1.56 V *vs*. RHE) for MOR in 1 M KOH + 1 M CH_3OH solution. The CA of Pt/C (20 wt%) was performed at a potential of -0.2 V *vs*. SCE (0.86 V *vs*. RHE) for MOR in 1 M KOH + 1 M CH_3OH solution. The anode catalyst loading of the Pt/C was 0.71 mg cm^{-2} including the mass of the carbon supports and the loading of the Pt was about 0.14 mg cm^{-2}.

To estimate the resistance to CO poisoning of $Ni(OH)_2/MnCO_3$ electrode, the chronoamperometry (CA) was performed at a potential of 0.5 V *vs*. SCE (1.56 V *vs*. RHE) for MOR in 1 M KOH + 1 M CH_3OH solution saturated with N_2 and CO. The CA of Pt/C was performed at a potential of -0.2 V *vs*. SCE (0.86 V *vs*. RHE) for MOR in 1 M KOH + 1 M CH_3OH solution saturated with N_2 and CO. Max normalization was employed to the chronoamperometric curves obtained in both N_2 and CO saturated solutions to demonstrate the extent of decay in the chronoamperometric curves in CO. This method allowed for a clear comparison by scaling the data

to a standardized range, highlighting the differences in curve attenuation under varying conditions. The formula for max normalization is: $x_{norm}=x/x_{max}$, where x is the original data point, x_{max} is the maximum value in the dataset, and x_{norm} is the normalized data point.

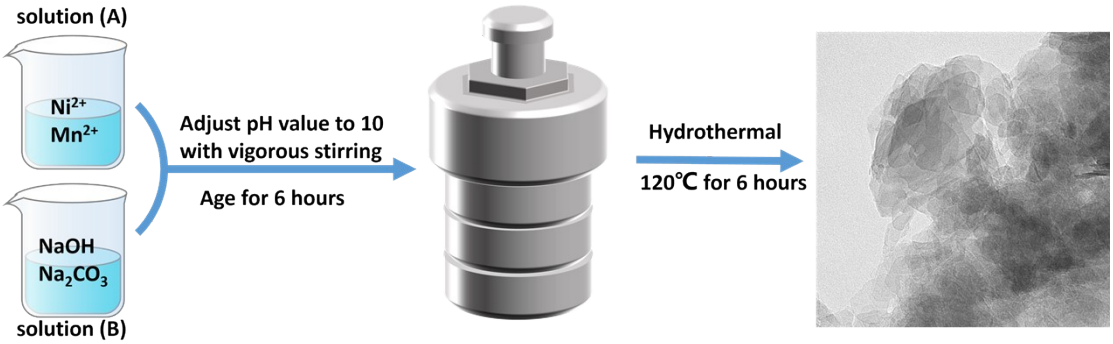

Figure S1. Schematic the synthetic route of $Ni(OH)_2/MnCO_3$ hybrid catalysts.

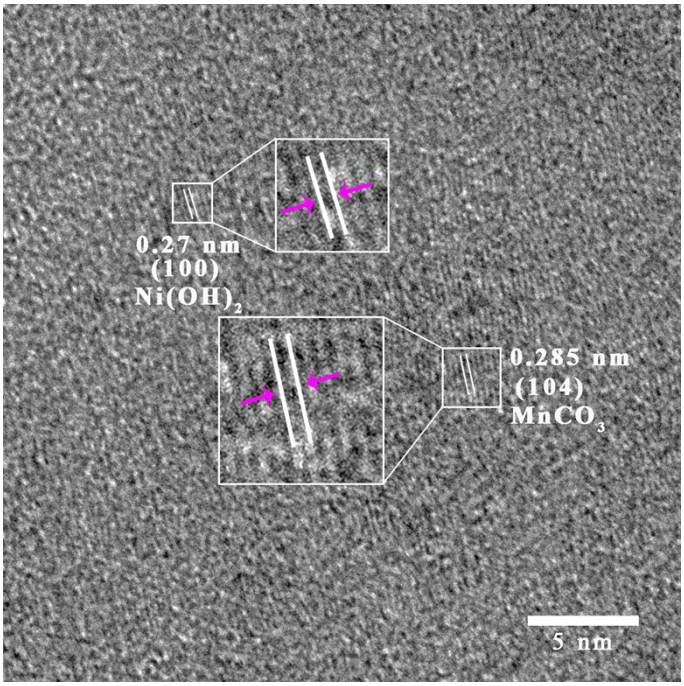

Figure S2. High-resolution image of $Ni(OH)_2/MnCO_3$(3:1) catalyst.

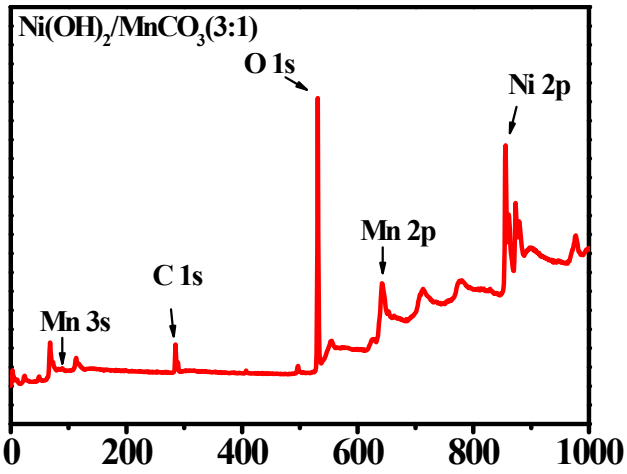

Figure S3. Full scan XPS spectra of $Ni(OH)_2/MnCO_3$ (3:1).

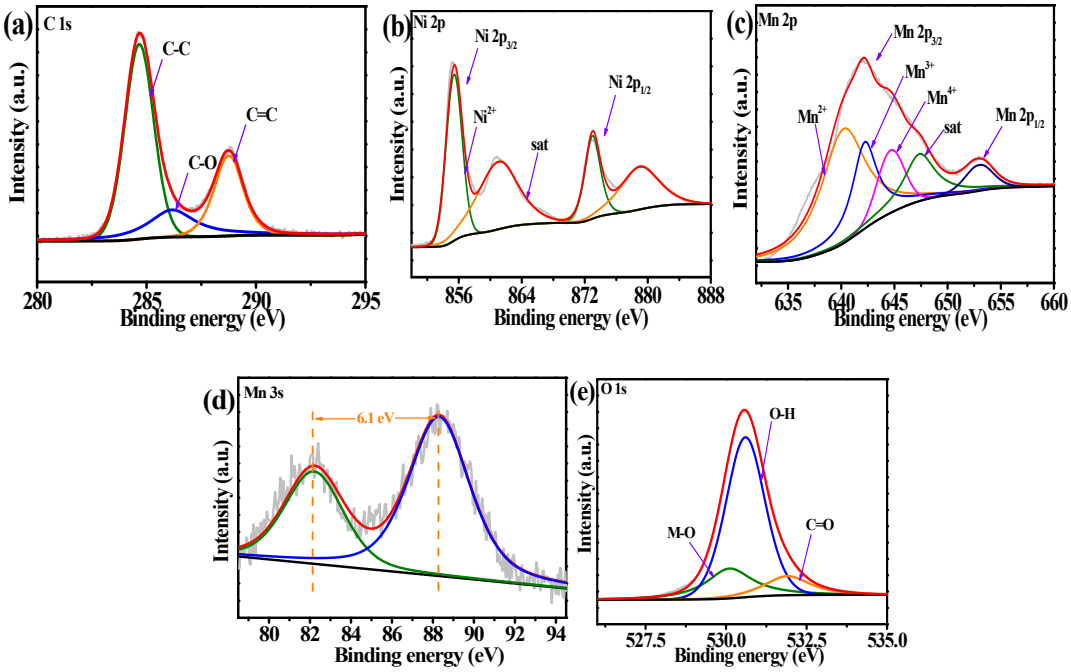

Figure S4. High-resolution XPS spectrum for C 1s (a), Ni 2p (b) and Mn 2p (c), Mn 3s (d) and O 1s (e) of $Ni(OH)_2/MnCO_3$(3:1).

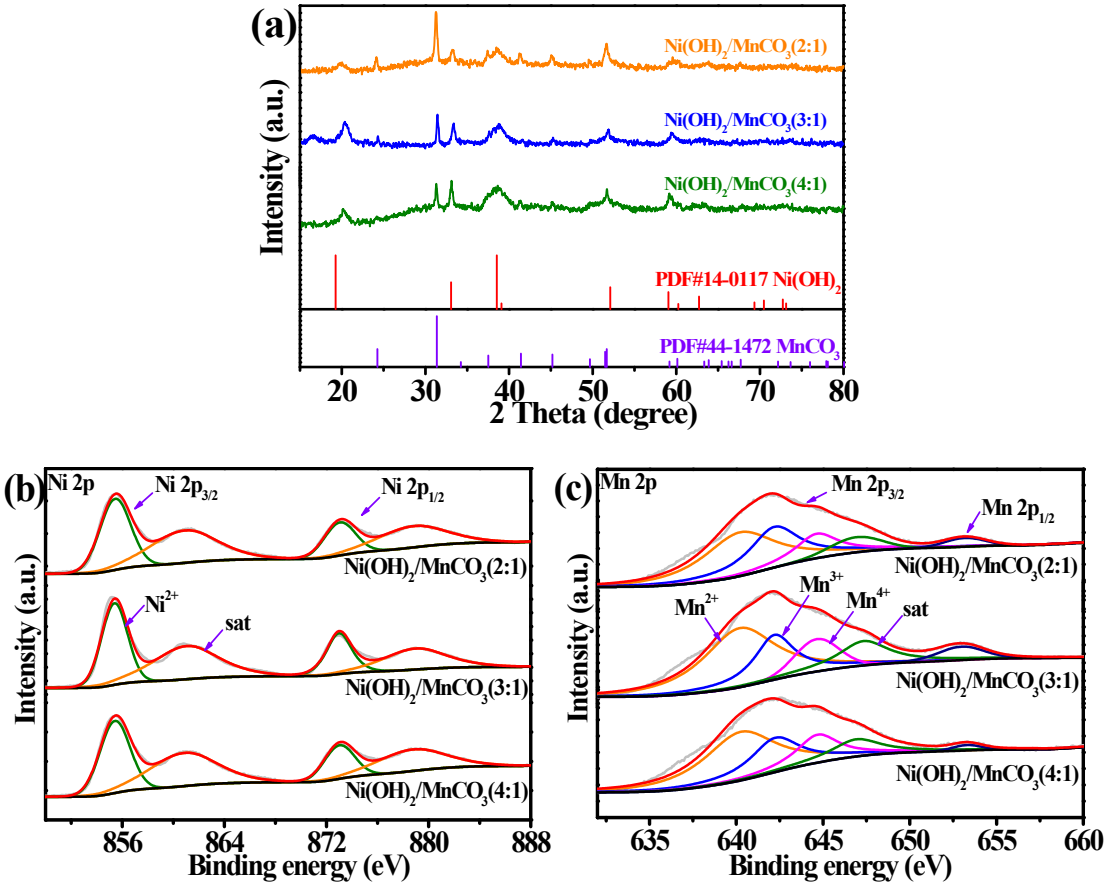

Figure S5. XRD pattern (a), high-resolution XPS spectrum for Ni 2p (b) and Mn 2p (c) of $Ni(OH)_2/MnCO_3$(2:1), $Ni(OH)_2/MnCO_3$(3:1) and $Ni(OH)_2/MnCO_3$(4:1).

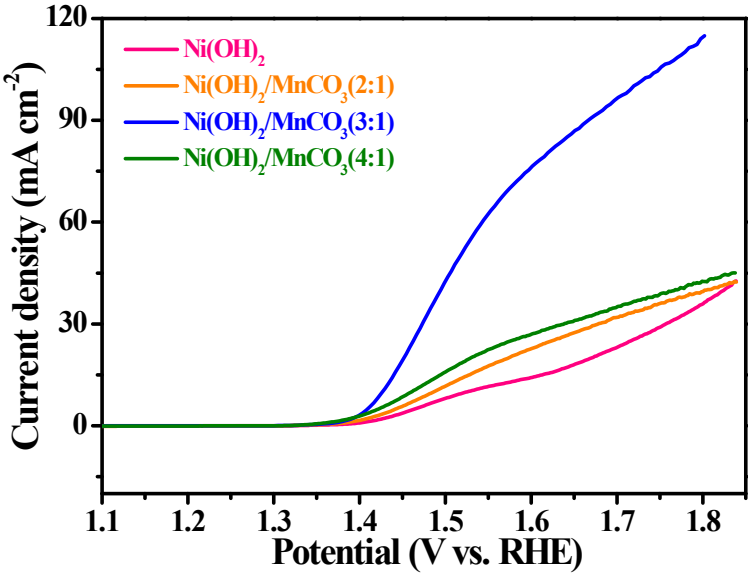

Figure S6. Linear sweep voltammetry curve of various catalysts at a scan rate of 5 mV s^{-1} with iR correction.

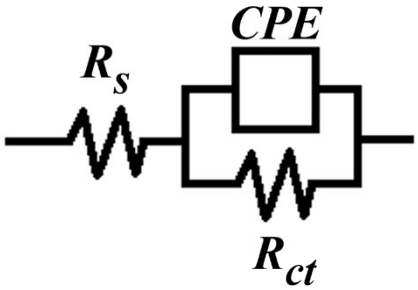

Figure S7. The equivalent circuit model was used to fit the Nyquist plots of EIS measurements. The equivalent circuit is composed of a resistor (*Rs*) and two parallel combinations including a charge-transfer resistance (*Rct*) and a constant phase element (*CPE*).

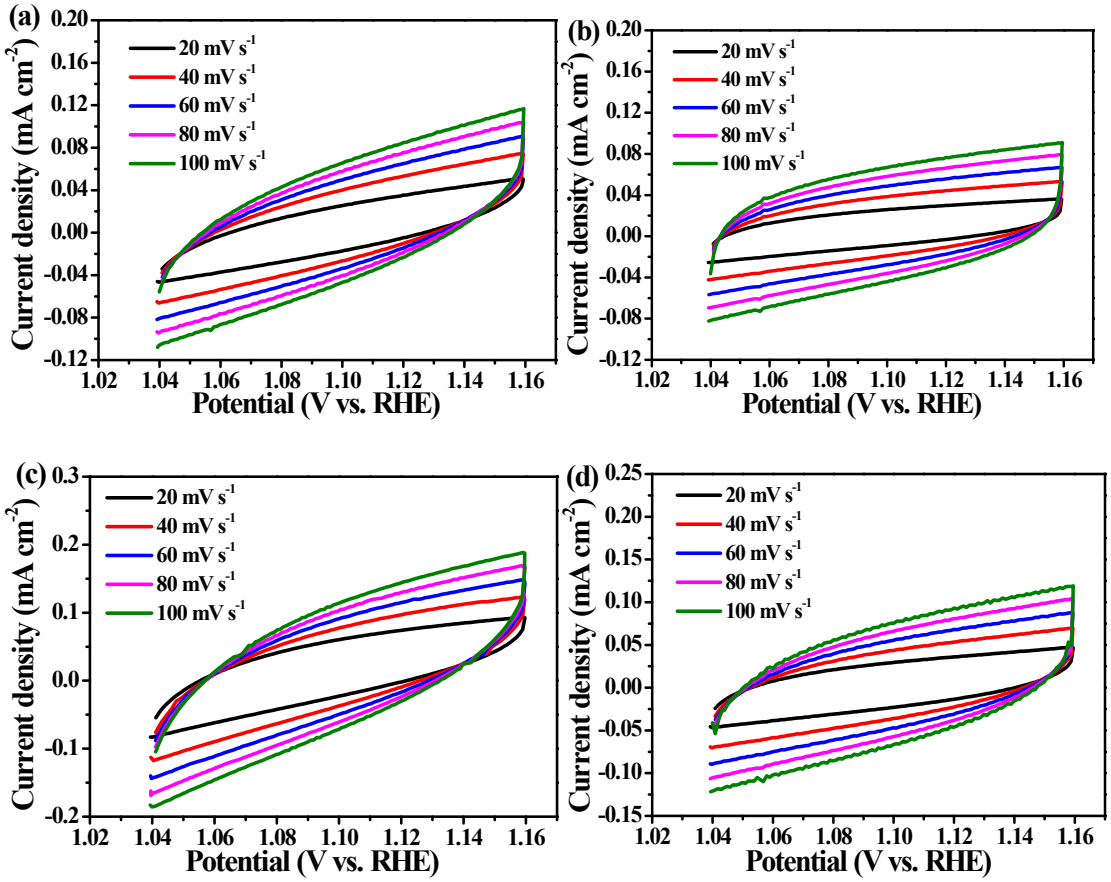

Figure S8. (a-d) Cyclic voltammograms for the double layer capacitance from -0.02 to 0.1 V *vs.* SCE (1.04 to 1.16 V *vs.* RHE) for $Ni(OH)_2$, $Ni(OH)_2/MnCO_3$ (2:1), $Ni(OH)_2/MnCO_3$ (3:1) and $Ni(OH)_2/MnCO_3$ (4:1).

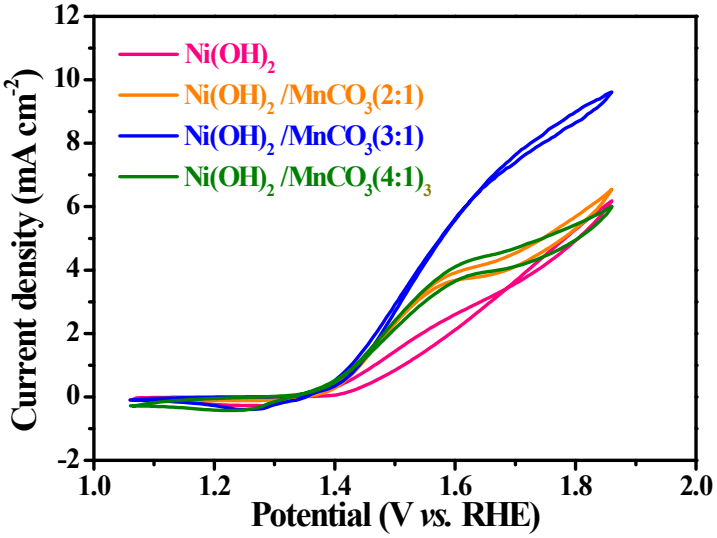

Figure S9. Specific activity curves of various catalysts for MOR.

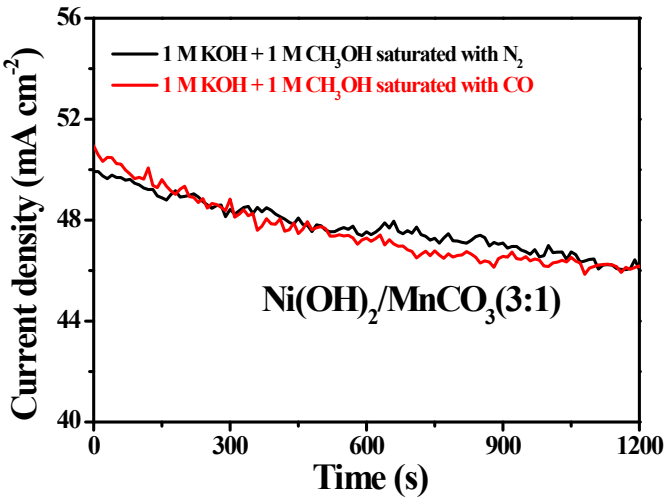

Figure S10. CA curves of $Ni(OH)_2/MnCO_3$(3:1) at 1.56 V vs. RHE in 1 M KOH + 1 M CH_3OH saturated with N_2 and CO.

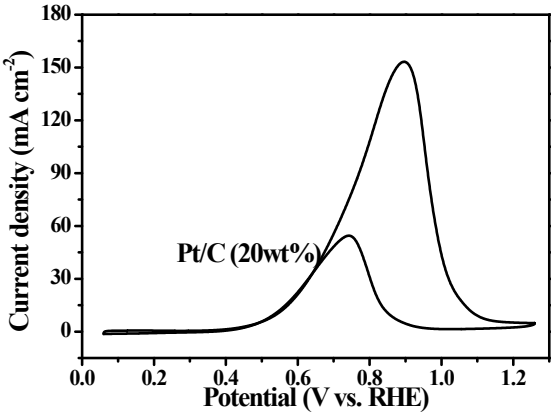

Figure S11. CV curve of Pt/C (20 wt%) in 1 M KOH + 1 M CH_3OH at a scan rate of 50 mV s^{-1}.

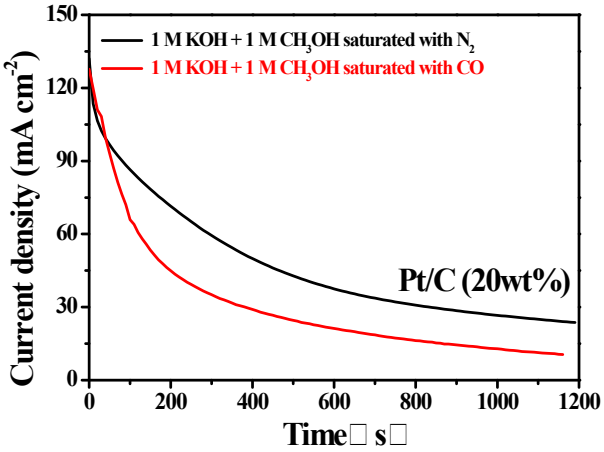

Figure S12. CA curves of Pt/C (20 wt%) at 0.86 V vs. RHE in 1 M KOH + 1 M CH_3OH saturated with N_2 and CO.

Table S1. Comparison of electrocatalytic performance of non-noble metal catalysts for MOR in alkaline media.

Catalysts	Electrolyte	Performance	Ref.
$Ni(OH)_2/MnCO_3$(3:1)	1M KOH + 1 M CH_3OH	149.7 mA cm^{-2} at 1.78 V vs. RHE 50 mA cm^{-2} at 1.49 V vs. RHE	This work
Ni-Cu/RCQDs/GCE	0.5 M KOH + 0.5 M CH_3OH	90.41 mA cm^{-2} at 0.72 V vs. Ag/AgCl (1.73 V vs. RHE)	[1]
$Ni_{60}Cr_{10}Ta_{10}P_{16}B_4$	1 M NaOH + 1 M CH_3OH	17.1 mA cm^{-2} at 0.75 V vs. Ag/AgCl (1.77 V vs. RHE)	[2]
$Ni_{2.5}Co_{0.5}Sn_2$	1 M KOH + 2 M CH_3OH	65 mA cm^{-2} at 0.6 V vs. Hg/HgO (1.53 V vs. RHE)	[3]
Ni-NiCu-3	0.1 M KOH + 1 M CH_3OH	28 mA cm^{-2} at 0.85 V vs. Hg/HgO (1.72 V vs. RHE)	[4]
Ni/Al LDH	1 M KOH + 2 M CH_3OH	25 mA cm^{-2} 0.55 V vs. SCE (1.61 V vs. RHE)	[5]
Ni/Fe LDH	1 M KOH + 2 M CH_3OH	40 mA cm^{-2} 0.55 V vs. SCE (1.61 V vs. RHE)	[5]
V_O-rich NiO	1 M KOH + 0.5 M CH_3OH	85.3 mA cm^{-2} at 0.7 V vs. Ag/AgCl (1.72 V vs. RHE)	[6]
NiS/CA	1 M KOH + 0.5 M CH_3OH	42.6 mA cm^{-2} at 0.8 V vs. Ag/AgCl (1.82 V vs. RHE)	[7]
$NiCo_2O_4$/rGO	1 M KOH + 0.5 M CH_3OH	78 mA cm^{-2} at 0.6 V vs. Ag/AgCl (1.62 V vs. RHE)	[8]
NiSe/RGO-550	1 M KOH + 0.5CH_3OH	59.84 mA cm^{-2} at 1.7 V vs.RHE	[9]
NiCoPO-2	0.5 M KOH + 1 M CH_3OH	39.9 mA cm^{-2} at 0.8 V vs.SCE (1.86 V vs. RHE)	[10]
$Co_{0.2}Ni_{0.2}$-Gr	1 M KOH + 3 M CH_3OH	230 mA cm^{-2} at 1 V vs.Ag/AgCl (2.02 V vs. RHE)	[11]

Table S2. The binding energy of Ni 2p and Mn 2p components for the $Ni(OH)_2/MnCO_3$(2:1), $Ni(OH)_2/MnCO_3$(3:1) and $Ni(OH)_2/MnCO_3$(4:1) catalysts.

Catalysts	Ni $2p_{3/2}$		Ni $2p_{1/2}$		*Mn* $2p_{3/2}$	
	Peak	**Binding energy (eV)**	**Peak**	**Binding energy (eV)**	**Peak**	**Binding energy (eV)**
$Ni(OH)_2/MnCO_3$(2:1)	Ni^{2+}	873.1	Ni^{2+}	855.5	Mn^{2+}	640.2
					Mn^{3+}	642.2
					Mn^{4+}	644.6
$Ni(OH)_2/MnCO_3$(3:1)	Ni^{2+}	873	Ni^{2+}	855.4	Mn^{2+}	640.2
					Mn^{3+}	642.2
					Mn^{4+}	644.6
$Ni(OH)_2/MnCO_3$(4:1)	Ni^{2+}	873	Ni^{2+}	855.4	Mn^{2+}	640.2
					Mn^{3+}	642.2
					Mn^{4+}	644.6

Table S3. EIS fitting parameters for different catalyst samples.

Sample	R_s/ Ω	R_{ct}/ Ω	CPE/ S S^{-n}	Chi-squared
$Ni(OH)_2$	8.4	518	1.882E-005	1.401E-02
$MnCO_3$	8.7	578	2.964E-005	3.500E-02
$Ni(OH)_2/MnCO_3$(2:1)	8.6	299	2.591E-005	1.035E-02
$Ni(OH)_2/MnCO_3$(3:1)	8.9	68	6.980E-005	3.100E-03
$Ni(OH)_2/MnCO_3$(4:1)	9.1	193	4.374E-005	7.874E-03

Table S4. The C_{dl}, ECSA and R_f values of $Ni(OH)_2$, $Ni(OH)_2/MnCO_3$(2:1), $Ni(OH)_2/MnCO_3$(3:1) and $Ni(OH)_2/MnCO_3$(4:1).

Sample	C_{dl}/ mF cm^{-2}	ECSA/ cm^2	R_f
$Ni(OH)_2$	0.41	0.73	10.46
$Ni(OH)_2/MnCO_3$(2:1)	0.46	0.805	11.5
$Ni(OH)_2/MnCO_3$(3:1)	0.62	1.09	15.56
$Ni(OH)_2/MnCO_3$(4:1)	0.55	0.963	13.75

Reference

[1] H. Javan, E. Asghari, H. Ashassi-Sorkhabi, Design of new anodic bimetallic nanocatalyst composed of Ni–Cu supported by reduced carbon quantum dots for the methanol oxidation reaction, Diamond Relat. Mater., 115 (2021) 108348.

[2] N. Boostani, S. Vardak, R. Amini, Z. Mohammadifard, Optimization of Ni-Co-metallic-glass powder ($Ni_{60}Cr_{10}Ta_{10}P_{16}B_4$) (MGP) nanocomposite coatings for direct methanol fuel cell (DMFC) applications, Int. J. Hydrog. Energy, 48 (2023) 10002-10015.

[3] J. Li, Z. Luo, F. He, Y. Zuo, C. Zhang, J. Liu, X. Yu, R. Du, T. Zhang, M.F. Infante-Carrió, P. Tang, J. Arbiol, J. Llorca, A. Cabot, Colloidal Ni–Co–Sn nanoparticles as efficient electrocatalysts for the methanol oxidation reaction, J. Mater. Chem. A, 6 (2018) 22915-22924.

[4] S. Liu, Y. Sun, Y. Wu, Y. Wang, Q. Pi, S. Li, Y. Li, D. Li, Common Strategy: Mounting the Rod-like Ni-Based MOF on Hydrangea-Shaped Nickel Hydroxide for Superior Electrocatalytic Methanol Oxidation Reaction, ACS Appl. Mater. Interfaces, 13 (2021) 26472-26481.

[5] Y. Vlamidis, S. Fiorilli, M. Giorgetti, I. Gualandi, E. Scavetta, D. Tonelli, Role of Fe in the oxidation of methanol electrocatalyzed by Ni based layered double hydroxides: X-ray spectroscopic and electrochemical studies, RSC Adv., 6 (2016) 110976-110985.

[6] W. Yang, X. Yang, J. Jia, C. Hou, H. Gao, Y. Mao, C. Wang, J. Lin, X. Luo, Oxygen vacancies confined in ultrathin nickel oxide nanosheets for enhanced electrocatalytic methanol oxidation, Appl. Catal. B: Environ., 244 (2019) 1096-1102.

[7] G. Hou, Z. Lyu, Y. Tang, H. Cao, G. Zheng, Preparation of flexible composite electrode with bacterial cellulose (BC)-derived carbon aerogel supported low loaded NiS for methanol electrocatalytic oxidation, Int. J. Hydrog. Energy, 45 (2020) 16049-16059.

[8] N. Narayanan, N. Bernaurdshaw, Reduced Graphene Oxide Supported $NiCo_2O_4$ Nano-Rods: An Efficient, Stable and Cost-Effective Electrocatalyst for Methanol Oxidation Reaction, ChemCatChem, 12 (2020) 771-780.

[9] J. Jia, L. Zhao, Y. Chang, M. Jia, Z. Wen, Understanding the growth of NiSe nanoparticles on reduced graphene oxide as efficient electrocatalysts for methanol oxidation reaction, Ceram. Int., 46 (2020) 10023-10028.

[10] Y.Y. Tong, C.D. Gu, J.L. Zhang, H. Tang, Y. Li, X.L. Wang, J.P. Tu, Urchin-like Ni-Co-P-O nanocomposite as novel methanol electro-oxidation materials in alkaline environment, Electrochim. Acta, 187 (2016) 11-19.

[11] N.A.M. Barakat, M. Motlak, Co_xNi_y-decorated graphene as novel, stable and super effective non-precious electro-catalyst for methanol oxidation, Appl. Catal. B: Environ., 154-155 (2014) 221-231.